Phys. Med. Biol. **43** (1998) 2431–2452. Printed in the UK PII: S0031-9155(98)91031-4

Measured molecular coherent scattering form factors of animal tissues, plastics and human breast tissue

Douglas E Peplow† and Kuruvilla Verghese
Department of Nuclear Engineering, NC State University, Raleigh, NC 27695-7909, USA

Received 23 January 1998, in final form 14 May 1998

Abstract. Photon scattering angular distributions from various animal tissues were measured at two energies of a monochromatic synchrotron x-ray beam. Two plastics and human breast tissue were also measured. From these two measurements, the molecular coherent scattering form factor of each material was extracted. A new data analysis technique that uses Monte Carlo based corrections for air scattering, incoherent scattering and multiple scattering was used. The form factors of the 16 materials are presented in tabular form, suitable for use in computer calculations.

1. Introduction

As part of a team studying a new mammographic imaging modality using linearly polarized monoenergetic photons (Chapman *et al* 1997, Johnston *et al* 1996), we are interested in performing some design analysis using Monte Carlo calculations. In order to simulate the radiographic image, both the coherent and incoherent angular scattering distributions must be known in detail.

Narten (1970) and Narten and Levy (1971) measured the scattering distribution of water at various temperatures. These measurements used a molybdenum tube source with a characteristic x-ray energy of 17.4 keV. Measurements of this type are expressed as functions of x, related to the momentum transfer of the interaction, $x = (E/hc)\sin(\theta/2)$ where E is the photon energy, h is Planck's constant, c is the speed of light and θ is the angle of scatter. Their measurements included data from $x = 0.4$ to $x = 12.7$ per nm. The value at $x = 0$ was calculated using thermodynamic properties of water.

Johns and Yaffe (1983) showed that the atomic form factors, which dominate the angular distribution for coherent scattering, do not correctly predict the angular scattering distribution for photons in water. They showed that the measured molecular form factor must be used in order to obtain a reasonable agreement between calculation and measurement. The most significant difference in the theoretical and measured coherent scattering distributions is that the peak of the measured data is not at an angle of zero degrees.

Kosanetzky *et al* (1987) used a powder diffraction machine with a cobalt anode to measure the scattering distributions of various pig tissues and several plastics used in the AAPM mammographic phantoms. They found that most tissues appeared similar to water in their coherent scattering distributions. The distributions obtained by this group cover only up to $x = 4.28$ per nm due to the low energy, 6.935 keV, of the characteristic x-ray used in the measurements.

† E-mail address: depeplow@eos.ncsu.edu

 © 1998 IOP Publishing Ltd

Evans *et al* (1991) measured the coherent scattering distribution in many tissues, including adipose, fibroglandular, benign tumour, carcinoma, fibrocystic disease/benign mammary dysplasia and blood. They used a copper anode x-ray tube source operating at 60 kVp for the measurements. The photon distribution was calculated to have a mean energy of 46 keV with a full width at half maximum of 18 keV. They only tabulated the angle of the main peak in the scattering distributions of each material. They did not tabulate the angular distribution.

Leliveld *et al* (1996) refer to a set of tables of molecular form factors made using the data from Kosanetzky *et al* (1987). Of course, these tables cover only a small range of x and have the influence of a tube source spectrum.

Tartari *et al* (1997b) presented the molecular form factors of Lucite and pork fat in tabular form. The measurements were made with a powder diffraction machine up to $x = 6.4$ per nm. Monte Carlo calculations were used to find transmission factors and self-absorption corrections but overall the analysis was simple (Tartari *et al* 1997a).

What is needed, by our group and by others modelling photon transport problems where coherent scattering becomes important, is a set of tables of molecular coherent scattering form factors that can be used in Monte Carlo calculations. This paper provides that for several animal tissues, two plastics and human breast tissue. The method used to obtain these tables, a unique approach using a combination of two monoenergetic measurements, is described here as well. The tables are evaluated at the same x values as the tables by Hubbell and Øverbø (1979) in order to make it easier for modellers to incorporate these data sets into their calculations.

2. Theory

The differential cross sections for coherent and incoherent scattering of polarized x-rays of energy E to scatter to polar angle θ and azimuthal angle ϕ (measured from the direction of polarization) from an atom with atomic number Z are

$$\frac{\mathrm{d}}{\mathrm{d}\Omega}\sigma_{\mathrm{coh}}(\theta,\phi,E) = r_{\mathrm{e}}^2(1-\sin^2\theta\cos^2\phi)F^2(x,Z) \tag{1}$$

$$\frac{\mathrm{d}}{\mathrm{d}\Omega}\sigma_{\mathrm{inc}}(\theta,\phi,E) = \frac{r_{\mathrm{e}}^2}{2}\left(\frac{\alpha'}{\alpha}\right)^2\left(\frac{\alpha'}{\alpha}+\frac{\alpha}{\alpha'}-2\sin^2\theta\cos^2\phi\right)S(x,Z) \tag{2}$$

where $F(x,Z)$ is the atomic form factor, $S(x,Z)$ is the incoherent scattering factor, x may be written as $(E/1.239\,852\ \text{keV nm})\sin(\theta/2)$, α is $E/m_{\mathrm{e}}c^2$, α' is $E'/m_{\mathrm{e}}c^2 = \alpha/[1+\alpha(1-\cos\theta)]$ and $r_{\mathrm{e}} = e^2/4\pi\epsilon_0 m_{\mathrm{e}}c^2$ is the classical electron radius. The charge of an electron is e, $m_{\mathrm{e}}c^2$ is the rest energy of an electron and ϵ_0 is the permittivity of free space. The total cross sections for elements can be found by integrating these distributions.

The coherent scattering form factor F and the incoherent scattering factor S account for the interference between the electrons of the atom. Non-relativistic values for F and S were tabulated for elements 1 to 100 by Hubbell *et al* (1975, 1977) and a set of relativistic form factors were tabulated by Hubbell and Øverbø (1979).

Our measurements were carried out using monochromatic synchrotron radiation. This beam of radiation is completely linearly polarized in the horizontal direction. For measurements in the vertical plane ($\phi = 90°$), the term $\cos^2\phi$ reduces to 0 in the above differential cross sections.

When considering a molecule, F_{mol}^2 is often calculated (Chan and Doi 1983) by adding the squares of the individual atomic form factors, weighted by their respective atomic abundances n_i. Correspondingly, the molecular incoherent scattering factor is calculated by

adding the atomic scattering factors, again weighted by the atomic abundances

$$F^2_{\mathrm{mol}}(x) = \sum_i n_i F^2(x, Z_i) \tag{3}$$

$$S_{\mathrm{mol}}(x) = \sum_i n_i S(x, Z_i). \tag{4}$$

For most composite materials, the atomic abundances are not known so the composite scattering factor can be expressed without knowing the molecular formula as

$$\frac{F^2_{\mathrm{mol}}(x)}{W} = \sum_i \frac{w_i}{M_i} F^2(x, Z_i) \tag{5}$$

where w_i is the mass fraction of element i, M_i is the atomic mass of element i and W the molecular weight. A similar expression can be written for $S_{\mathrm{mol}}(x)/W$.

Since each atom is considered without regard to its neighbours, this is called the 'free-gas' model. This, however, does not include intramolecular effects or intermolecular effects caused by the close spacing of molecules in real materials. The use of atomic form factors for real materials is not adequate at low energies and/or small scattering angles. For accurate results, $F_{\mathrm{mol}}(x)$ must be measured. Amorphous materials such as plastics and water show broad peaks oscillating around the free-gas model. For strongly ordered materials such as crystals, the free-gas model completely breaks down and the true molecular form factor would be essentially zero for most values of x with many sharp diffraction peaks, corresponding to the crystal lattice planes.

At large values of x (i.e. either high energies or large scatter angles) the free-gas model and the true molecular coherent scattering form factor become the same. This fact is exploited in the extraction of the form factors from scattering data.

3. Methods

3.1. Samples

A total of 16 samples were measured for this study. These were: plastics commonly used in phantoms (Lucite and Lexan), Kapton, deionized water, five pork samples, five beef samples, formaline (10% formaldehyde in water) and human breast tissue fixed in formaline. Fresh pork and beef tissues were used due to the difficulty of obtaining fresh human tissues. These samples were kept refrigerated and never frozen. They were allowed to warm up to room temperature before measurement. The human breast tissue was fixed in formaline and stored at room temperature. A sample of formaline was measured as a check—to ensure that the measurement of the breast tissue was not just measuring formaline. Kapton was measured so that its effects could be removed from measurements of tissues that were held by a Kapton foil.

3.2. Scattering distribution measurement

Measurements of the angular scattering distributions were made on line X3B1 of the National Synchrotron Light Source at Brookhaven National Laboratory. This beamline can produce a monoenergetic beam from 5 keV to 30 keV with a full width at half maximum of less than 6 eV at 9 keV. The beam is nearly parallel and very close to completely polarized.

The beam size was 8 mm horizontal by 2 mm vertical. Between the sample and the detector was a set of Söller slits which allowed only a range of about 0.03° around the desired scatter angle to reach the detector. An NaI detector was used with only minimal

energy discrimination, allowing both coherent and incoherent scatter to be fully counted at any angle.

Tissue samples and liquids were contained in a plastic sample holder (Lucite) with a thin Kapton cover. The container was placed in the beam with the Kapton film at the centre of rotation. The sample size was $2.54 \times 1.91 \times 0.95$ cm. Measurements were made in reflection mode, with the sample container at an angle $\theta/2$ when the detector was at angle θ, as shown in figure 1. As seen in the figure, at low angles the side walls of the container would be in the beam, contributing scatter into the detector.

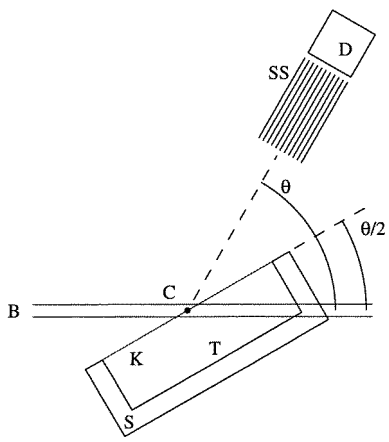

Figure 1. Cross-sectional view of the sample container in reflection mode. Tissue (T) is held by the sample container (S) and the Kapton foil (K). The monoenergetic beam of photons (B) from the synchrotron enter from the left. The sample container is rotated to an angle $\theta/2$ about the centre of rotation (C). This configuration is used to measure the scattering at angle θ, where the Söller slits (SS) and the detector (D) are positioned.

Solid samples (plastics and Kapton) were measured in transmission mode, which was less susceptible to alignment errors. The samples were held at angle $\theta/2$ when the detector was at angle θ to reduce the attenuation thickness and maximize signal to the detector. Every sample was measured at two different x-ray energies. Lexan and Lucite were measured at a thickness of 1.59 cm for the high-energy run, and for the low-energy run 0.16 cm was used.

The choice of beam energy affects the range of x that is measured. To provide data at large x where the atomic form factor calculation matches molecular form factor calculations, a high beam energy is required. But at this higher beam energy, the interesting details in the molecular form factor are crowded down in the low-x range, where low-angle geometry effects appear. Using a low beam energy will move the interesting details away from the geometry effects but will not provide the data at large x. For these reasons, both high- and low-energy beams were used and the results were combined in the final determination of the form factors.

Measurements of the scattered x-rays from the samples were made at 20 keV at intervals of 0.25° for angles from 1° to 110° resulting in a range of x from 0.14 to 13 per nm. The low-energy measurements were made at 8 keV at every 0.25° from 1° to 60° ($x = 0.056$ to 3.2 per nm). A computer precisely controlled the motion of the sample and the detector and also collected the data. Data collection times varied from 20 min to 2 h, depending on the beam energy and synchrotron photon flux. The data were corrected for detector dead time

and the synchrotron photon flux, which decayed with ring current. Except for Kapton, data were collected to a statistical uncertainty ($1/\sqrt{\text{counts}}$) of less than 1%. Kapton, which was a very thin sample, had an average uncertainty of 4% and 2% respectively for the 20 keV and 8 keV photon energies.

3.3. Data analysis procedure

The analysis is based on the fact that the oscillations in the molecular form factor damp out at high x values. A Monte Carlo calculation using atomic form factors should match the measured data in this high x-range. Once the model and the data are fitted, the molecular form factor can be extracted from the data. The effects of the sample holder, Kapton cover and air can also be accounted for in the model and then subtracted out of the data. This procedure uses both the high-energy and low-energy measurements to provide more details in the low-x region.

Modelling the entire response expected from radiation scattered from anywhere in the experiment is a much more rigorous approach than reported in the literature (Kosanetzky *et al* 1987, Tartari *et al* 1997b). Attempting to subtract the measured scattering distribution of an empty sample container from the scattering distribution of a container plus sample is inaccurate since this problem is definitely not linear.

3.3.1. Solid samples. First the Lucite, Lexan and Kapton samples were analysed since their molecular form factors would be needed in the Monte Carlo simulations of the sample holder which held the tissues. The first step in extracting a molecular form factor from a data set was to perform a Monte Carlo calculation of the expected response using the atomic form factors in a free-gas model. This was done using an in-house code. The code has been compared with both Chan and Doi (1983) and Boone (1992) and found to match their results well. The Monte Carlo code followed particles through the geometry and at each interaction site calculated the probability of coherent and incoherent scatter through the Söller slits and into the detector. The model calculated the expected response at the same angles that were used in the experimental measurements.

For these three samples, x-ray interactions in only two materials were considered: the sample and the surrounding air. The response was tabulated into different tallies depending on the type of scatter (coherent or incoherent) and which material was the scatterer. A tally was also kept for multiple scatter, which included any photon that was scattered more than once in any combination of materials.

The total Monte Carlo predicted response, R, at each angle was then

$$R = C_{\text{sam}} + C_{\text{air}} + I_{\text{sam}} + I_{\text{air}} + M \tag{6}$$

where C_i and I_i represent the amount of coherent and incoherent single scatter respectively from material i (sample or air) and M represents the multiple scatter component. What the Monte Carlo code actually calculated was

$$C_i = \int_V \exp(-\mu s_1) \frac{\rho_i N_A}{W_i} r_{\text{e}}^2 F_i^2(x) \exp(-\mu s_2)\, \mathrm{d}V \tag{7}$$

$$I_i = \int_V \exp(-\mu s_1) \frac{\rho_i N_A}{W_i} r_{\text{e}}^2 \left(\frac{\alpha'}{\alpha}\right)^2 \left(\frac{\alpha'}{\alpha} + \frac{\alpha}{\alpha'}\right) S(x, Z) \exp(-\mu' s_2)\, \mathrm{d}V \tag{8}$$

at each scatter angle where μ and μ' represent the attenuation coefficients for the entering and exiting photon, s_1 and s_2 the lengths of the entrance path and exit path and V the volume of region i. N_A is Avogadro's number, ρ_i is the density of material i and W_i is the

molecular weight of material i. Since the Söller slits allowed only one scatter angle to be detected, the first integral was reduced to

$$C_i = r_e^2 \frac{\rho_i N_A}{W} F_i^2(x) \int_V \exp(-\mu s_1) \exp(-\mu s_2)\, \mathrm{d}V \tag{9}$$

$$= F_i^2(x) G_i \tag{10}$$

where G_i contains the information about the geometry, the self-attenuation correction and the constant term. The two single scatter components calculated by the Monte Carlo code completely matched the analytic forms of equations (7) and (8).

The Monte Carlo calculation for 20 keV photons, R_{20}, was fit by linear least squares to the experimental data, D_{20}, in the region $x = 9$ to 13 per nm

$$D_{20} = a_1 R_{20} \tag{11}$$

$$= a_1 (C_{\mathrm{sam}} + C_{\mathrm{air}} + I_{\mathrm{sam}} + I_{\mathrm{air}} + M) \tag{12}$$

to find the coefficient a_1. Once a_1 was fixed, the experimental data were then set equal to the coherent scatter term using the true molecular form factor, $F_{\mathrm{mol},20}$, plus all of the other calculated components.

$$D_{20} = a_1 (F_{\mathrm{mol},20}^2(x) G_{\mathrm{sam}} + C_{\mathrm{air}} + I_{\mathrm{sam}} + I_{\mathrm{air}} + M). \tag{13}$$

Of course, the G_{sam} was easily found by dividing the Monte Carlo data by the square of the atomic form factor, $C_{\mathrm{sam}}/F_{\mathrm{sam}}^2$. Inserting this and solving for the molecular form factor gave

$$D_{20} = a_1 \left(F_{\mathrm{mol},20}^2(x) \frac{C_{\mathrm{sam}}}{F_{\mathrm{sam}}^2(x)} + C_{\mathrm{air}} + I_{\mathrm{sam}} + I_{\mathrm{air}} + M \right) \tag{14}$$

$$F_{\mathrm{mol},20}^2(x) = \frac{F_{\mathrm{sam}}^2(x)}{C_{\mathrm{sam}}} \left(\frac{D_{20}}{a_1} - C_{\mathrm{air}} - I_{\mathrm{sam}} - I_{\mathrm{air}} - M \right). \tag{15}$$

This was now an approximation to the molecular form factor of the sample.

To get more detail in the low-x region, the process was repeated with the 8 keV data, D_8, and 8 keV Monte Carlo run, R_8. The data were fitted to the Monte Carlo responses except for the term C_{sam}, where the approximate form factor was used in place of the atomic form factor that was used in the calculation

$$D_8 = a_2 R_8 \tag{16}$$

$$= a_2 \left(C_{\mathrm{sam}} \frac{F_{\mathrm{mol},20}^2(x)}{F_{\mathrm{sam}}^2(x)} + C_{\mathrm{air}} + I_{\mathrm{sam}} + I_{\mathrm{air}} + M \right). \tag{17}$$

The fit was over the highest portion of the 8 keV data, $x > 0.275$, to find a_2. Once this was found, the molecular form factor was found by

$$D_8 = a_2 \left(F_{\mathrm{mol},8}^2(x) \frac{C_{\mathrm{sam}}}{F_{\mathrm{sam}}^2(x)} + C_{\mathrm{air}} + I_{\mathrm{sam}} + I_{\mathrm{air}} + M \right) \tag{18}$$

$$F_{\mathrm{mol},8}^2(x) = \frac{F_{\mathrm{sam}}^2(x)}{C_{\mathrm{sam}}} \left(\frac{D_8}{a_2} - C_{\mathrm{air}} - I_{\mathrm{sam}} - I_{\mathrm{air}} - M \right). \tag{19}$$

The values of $F_{\mathrm{mol},8}$ at low x were combined with values of $F_{\mathrm{mol},20}$ at high x to generate the final molecular form factor.

3.3.2. Liquids and tissue samples. The analysis of the other samples followed a similar procedure to that of the solid samples. The difference was that there were four materials to consider in the Monte Carlo calculation: the sample itself, the Lucite sample container, the Kapton cover and the surrounding air. The Monte Carlo calculations used the molecular form factors for the Lucite and Kapton and used atomic form factors for the sample and for air. Compositions for the various animal tissues were assumed to correspond to human tissue compositions, taken from ICRU Report 46 (ICRU 1992). An example of the tallies from the Monte Carlo calculation for water at 8 keV is shown in figure 2. As seen in the figure, multiple scatter is 10–20% of the total detected. For 20 keV, multiple scatter is about 6–9% of the total.

The 20 keV Monte Carlo response, R_{20}, was fitted to the 20 keV experimental data, D_{20}, over the range $x = 9$ to 13 per nm to find the fit coefficient a_1. This fit for water is shown in figure 3(a). The data were then set equal to the Monte Carlo responses from the other regions (i) plus a coherent scattering term containing the molecular form factor of the

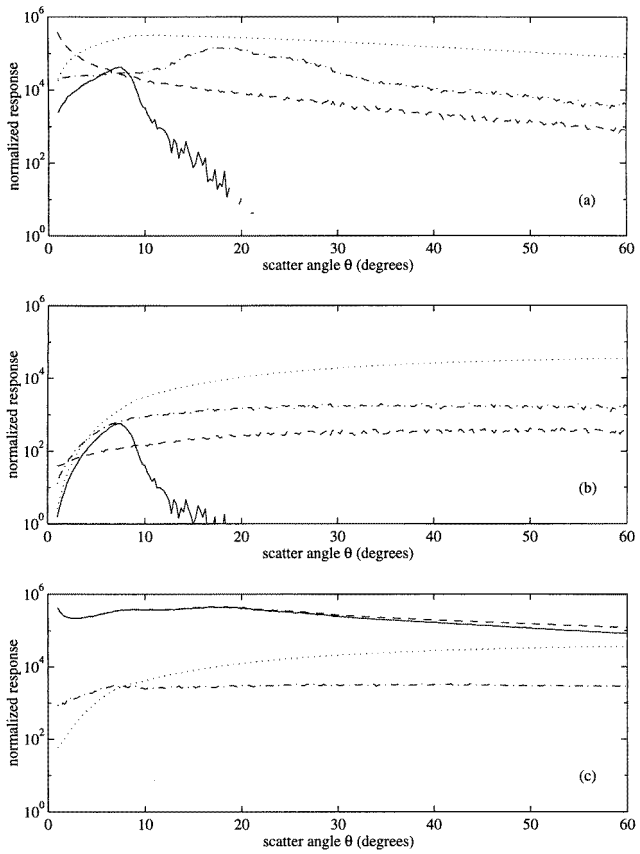

Figure 2. Monte Carlo predicted response for water using atomic form factors at 8 keV showing (a) single coherent scatter from the water (·····), the Kapton foil (— · —), the surrounding air (– – –) and the sample holder (——); (b) single incoherent scatter from the water (·····), the Kapton foil (— · —), the surrounding air (– – –) and the sample holder (——); and (c) the grand total (– – –), total coherent (——), total incoherent (·····) and multiple scatter (— · —).

sample (j). The molecular form factor was then found

$$D_{20} = a_1\left(F^2_{\mathrm{mol},20}(x)\frac{C_j}{F_j^2(x)} + \sum_{i\neq j} C_i + \sum_{i=1}^{4} I_i + M\right) \tag{20}$$

$$F^2_{\mathrm{mol},20}(x) = \frac{F_j^2(x)}{C_j}\left(\frac{D_{20}}{a_1} - \sum_{i\neq j} C_i - \sum_{i=1}^{4} I_i - M\right). \tag{21}$$

The approximate molecular form factor from the 20 keV data for water is shown in figure 3(b). As seen in the figure, most of the interesting details are in the range of $x < 3$ per nm. These details are difficult to extract due to the peak from the sample holder, which occurs at low angles, independent of the photon energy.

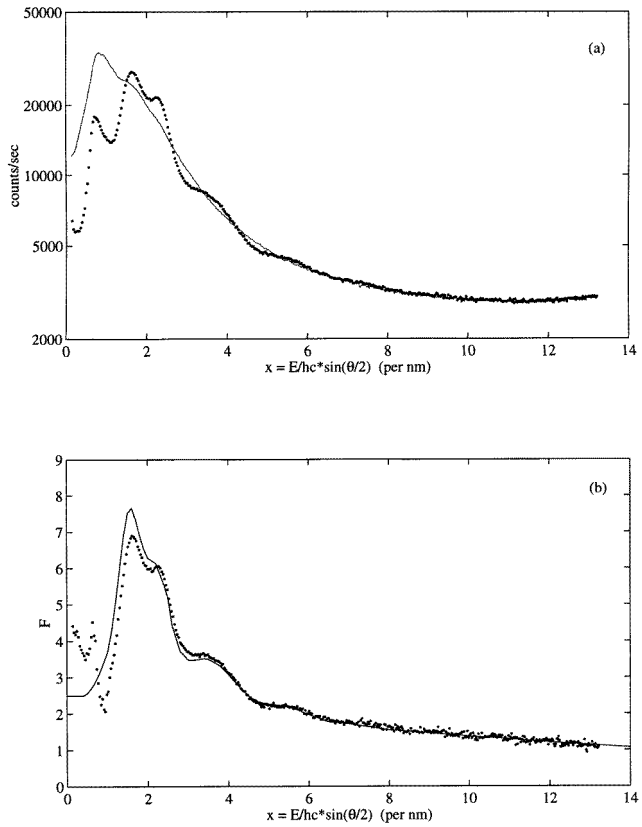

Figure 3. The extraction process (data shown here are for water): (a) the Monte Carlo calculation (——) using atomic form factors and the 20 keV data (·) for $x = 9$ to 13 per nm. (b) An approximation of the molecular form factor (·) as described in the text and Narten's data (1970) using a polyenergetic source (——).

Also shown in figure 3(b) is Narten's measured molecular form factor for 25 °C water. It is apparent from this figure that the scattering from the sample container and the air was not completely accounted for in the process of obtaining the form factor. Slight variations in alignment and slight curvatures of the Kapton foil too small to be taken into account in the Monte Carlo model are the causes. This was confirmed by experiment (forcing large curvatures in the Kapton) and by multiple Monte Carlo runs (beam alignment changes).

Reiterating, to provide more details at the low-x range, the 8 keV data were used. First, the coherent scatter tally from the sample (region j) was modified by the approximate molecular form factor found from the 20 keV data. Using this and all of the other tallies (i), a fit coefficient, a_2, was found. The 8 keV fit for water is shown in figure 4(a). The molecular form factor was then extracted by

$$D_8 = a_2\left(F^2_{\mathrm{mol},8}(x)\frac{C_j}{F_j^2(x)} + \sum_{i\neq j} C_i + \sum_{i=1}^{4} I_i + M\right) \tag{22}$$

$$F^2_{\mathrm{mol},8}(x) = \frac{F_j^2(x)}{C_j}\left(\frac{D_8}{a_2} - \sum_{i\neq j} C_i - \sum_{i=1}^{4} I_i - M\right). \tag{23}$$

The molecular form factor $F_{\mathrm{mol},8}$ for water is also shown in figure 4(b) with Narten's measurement. As with the solid samples, the values of $F_{\mathrm{mol},8}$ at low x were combined with values of $F_{\mathrm{mol},20}$ at high x to generate the final molecular form factor.

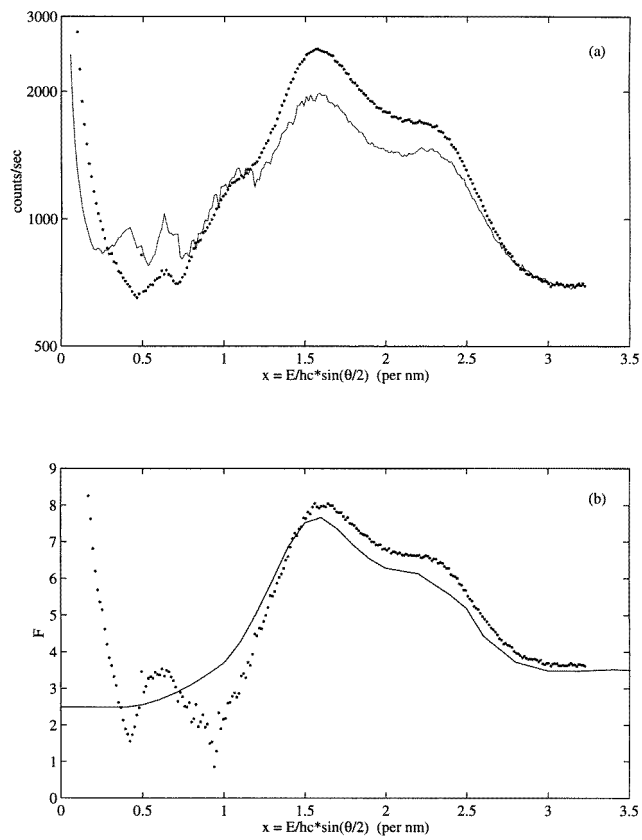

Figure 4. The extraction process continued (data shown here are for water): (a) the 8 keV Monte Carlo calculation (——), modified by the approximate form factor from the 20 keV data, and the 8 keV measured data (·) for $x > 2.75$ per nm. (b) Form factor using both the 8 and 20 keV data and Narten's molecular form factor (——).

3.4. Extrapolation at very low x

After obtaining the form factors from a few samples, it was noticed that the fit at low angles was not good. Again, this is believed to be caused by small alignment errors, slight curvatures in the sample holder cover and effects of the primary beam from the synchrotron which were not modelled. To remedy this, one of two approaches was used. The first approach replaced the tainted values at low x with Narten's (1970) value for water at $x = 0$, which was calculated from bulk thermodynamic principles. Narten's value was used up to some x_{crit} corresponding to the rise of the main peak. This method was used for most of the tissues, since they consist mostly of water and their distributions appear similar to water. The second approach simply used the lowest value of F before the drastic rise near $x = 0$ from air scatter. From $x = 0$ to some x_{crit}, where F is a minimum, the value of $F(x_{\mathrm{crit}})$ was used. This method was used for the plastics, adipose and breast tissue. Examples of each method are shown in figure 5. Table 1 lists each sample and which approach was used.

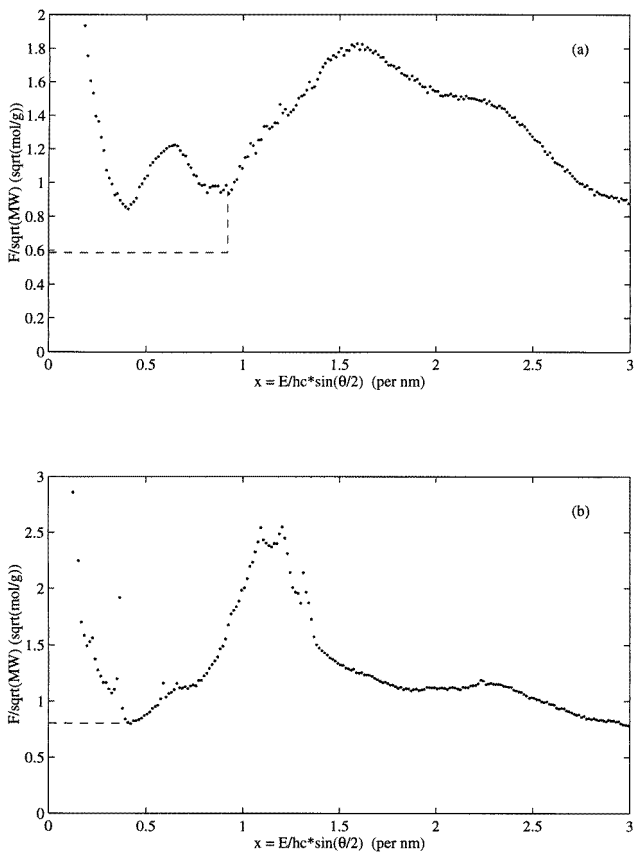

Figure 5. Example of extrapolation at very low x values: (a) the calculated value of water for water based tissues (this example is beef liver) or (b) the lowest value in the low-x region for non-water based materials (this example is pork adipose). The extrapolations are shown as (- - - -).

Table 1. Method of extrapolation to $x = 0$ and relative error of the final molecular form factor F_{mol}.

	Low-x extrapolation		Relative error in F	
Sample material	Method	x_{crit} (per nm)	Highest	Average
Lucite	Low point	0.18	0.049	0.013
Lexan	Low point	0.15	0.053	0.013
Kapton	Low point	0.32	0.344	0.044
Water	Water value	1.01	0.048	0.017
Pork adipose	Low point	0.42	0.053	0.015
Beef adipose	Low point	0.42	0.051	0.015
Pork muscle	Water value	0.92	0.048	0.013
Beef muscle	Water value	0.92	0.046	0.013
Pork kidney	Water value	0.92	0.360	0.015
Beef kidney	Water value	0.92	0.053	0.014
Pork liver	Water value	0.92	0.039	0.014
Beef liver	Water value	0.92	0.042	0.014
Pork heart	Water value	0.93	0.064	0.014
Beef blood	Water value	1.08	0.047	0.017
Human breast tissue	Low point	0.42	1.118	0.067
Formaline	Water value	0.99	0.052	0.017

3.5. Molecular form factor tables

In order to make the molecular form factors useful, they have been interpolated and tabulated at the same x values as the tables by Hubbell and Øverbø (1979). The form factors were smoothed using a five point average in the range of $x = 5$ to 10 per nm. Four examples are shown in figure 6. Hubbell and Øverbø's relativistic atomic form factors, combined using the free-gas approximation, are used in the tables above $x = 10$ per nm. By interpolating values of the molecular form factors only at the x values of Hubbell and Øverbø, some fine details seen in the figures in this paper will be missed.

Units of the table are the form factor per square root of molecular weight. This was used since the tissues have no molecular formula to speak of, only a composition by mass fractions. Individual users have probably found different ways to handle this and the units of the table should fit everyone. The values are all listed in tables 2–4. Table 1 lists the highest relative error in the form factor and the average relative error over the range of $x = x_{crit}$ to 10 per nm for each sample. This error takes into account the counting statistics from the high- and low-energy measurements and the stochastic error from the high- and low-energy Monte Carlo calculations.

The tables shown in this paper and a set of more detailed tables may be obtained from the first author, through his web site at `http://www4.ncsu.edu/~depeplow`.

4. Results and discussion

The molecular form factor of water is compared with Narten's measurement in figure 6(b). The peak in our form factor is sharper, possibly due to the use of a monoenergetic beam instead of a tube source. The close agreement of the two curves implies that the measurements and data analysis of the other tissues are valid.

The form factors of the animal tissues all appear similar in shape to water. This is consistent with the composition of these tissues. The adipose tissue from pork and

Table 2. Molecular coherent scattering form factors.

x (per nm)	Lucite	Lexan	Kapton	Water
0.00E + 00	0.9220E + 00	0.9827E + 00	0.8556E + 00	0.5871E + 00
0.10E + 00	0.9220E + 00	0.9827E + 00	0.8556E + 00	0.5871E + 00
0.20E + 00	0.9367E + 00	0.9881E + 00	0.8556E + 00	0.5871E + 00
0.30E + 00	0.1018E + 01	0.1052E + 01	0.8556E + 00	0.5871E + 00
0.40E + 00	0.1188E + 01	0.1134E + 01	0.9293E + 00	0.5871E + 00
0.50E + 00	0.1486E + 01	0.1169E + 01	0.1013E + 01	0.5871E + 00
0.60E + 00	0.1861E + 01	0.1187E + 01	0.1200E + 01	0.5871E + 00
0.70E + 00	0.2340E + 01	0.1403E + 01	0.1485E + 01	0.5871E + 00
0.80E + 00	0.2419E + 01	0.1814E + 01	0.2161E + 01	0.5871E + 00
0.90E + 00	0.2173E + 01	0.2434E + 01	0.2658E + 01	0.5871E + 00
0.10E + 01	0.1902E + 01	0.2498E + 01	0.3095E + 01	0.5871E + 00
0.11E + 01	0.1633E + 01	0.2225E + 01	0.3156E + 01	0.7338E + 00
0.12E + 01	0.1430E + 01	0.1855E + 01	0.2939E + 01	0.1048E + 01
0.13E + 01	0.1287E + 01	0.1592E + 01	0.2671E + 01	0.1299E + 01
0.14E + 01	0.1256E + 01	0.1508E + 01	0.2581E + 01	0.1568E + 01
0.15E + 01	0.1314E + 01	0.1423E + 01	0.2483E + 01	0.1800E + 01
0.16E + 01	0.1389E + 01	0.1285E + 01	0.2104E + 01	0.1876E + 01
0.17E + 01	0.1414E + 01	0.1167E + 01	0.1786E + 01	0.1840E + 01
0.18E + 01	0.1352E + 01	0.1080E + 01	0.1576E + 01	0.1758E + 01
0.19E + 01	0.1263E + 01	0.1001E + 01	0.1405E + 01	0.1667E + 01
0.20E + 01	0.1146E + 01	0.9553E + 00	0.1395E + 01	0.1600E + 01
0.22E + 01	0.1105E + 01	0.9808E + 00	0.1274E + 01	0.1560E + 01
0.24E + 01	0.1084E + 01	0.1021E + 01	0.1191E + 01	0.1451E + 01
0.25E + 01	0.9855E + 00	0.1019E + 01	0.1199E + 01	0.1324E + 01
0.26E + 01	0.8875E + 00	0.9694E + 00	0.1168E + 01	0.1167E + 01
0.28E + 01	0.7845E + 00	0.8165E + 00	0.1087E + 01	0.9384E + 00
0.30E + 01	0.7317E + 00	0.6919E + 00	0.9445E + 00	0.8699E + 00
0.32E + 01	0.6827E + 00	0.6273E + 00	0.9224E + 00	0.8600E + 00
0.34E + 01	0.6389E + 00	0.5743E + 00	0.8561E + 00	0.8571E + 00
0.35E + 01	0.6291E + 00	0.5660E + 00	0.8222E + 00	0.8515E + 00
0.36E + 01	0.6128E + 00	0.5620E + 00	0.7401E + 00	0.8305E + 00
0.38E + 01	0.6042E + 00	0.5796E + 00	0.7278E + 00	0.8022E + 00
0.40E + 01	0.5959E + 00	0.6126E + 00	0.7754E + 00	0.7354E + 00
0.42E + 01	0.5978E + 00	0.6293E + 00	0.7684E + 00	0.6701E + 00
0.44E + 01	0.6190E + 00	0.6292E + 00	0.8115E + 00	0.6150E + 00
0.45E + 01	0.6137E + 00	0.6184E + 00	0.7909E + 00	0.5769E + 00
0.46E + 01	0.6016E + 00	0.5949E + 00	0.7741E + 00	0.5558E + 00
0.48E + 01	0.5492E + 00	0.5743E + 00	0.7583E + 00	0.5226E + 00
0.50E + 01	0.5056E + 00	0.5401E + 00	0.7050E + 00	0.5222E + 00
0.55E + 01	0.4645E + 00	0.4643E + 00	0.6283E + 00	0.5166E + 00
0.60E + 01	0.4549E + 00	0.4500E + 00	0.5848E + 00	0.4744E + 00
0.65E + 01	0.4707E + 00	0.4513E + 00	0.5443E + 00	0.4316E + 00
0.70E + 01	0.4492E + 00	0.4605E + 00	0.5067E + 00	0.4196E + 00
0.80E + 01	0.4119E + 00	0.4225E + 00	0.4592E + 00	0.3793E + 00
0.90E + 01	0.3534E + 00	0.3716E + 00	0.4369E + 00	0.3522E + 00
0.10E + 02	0.3160E + 00	0.3169E + 00	0.3190E + 00	0.3244E + 00
0.11E + 02	0.2912E + 00	0.2904E + 00	0.2925E + 00	0.3058E + 00
0.12E + 02	0.2674E + 00	0.2649E + 00	0.2671E + 00	0.2877E + 00
0.13E + 02	0.2448E + 00	0.2408E + 00	0.2431E + 00	0.2698E + 00
0.14E + 02	0.2234E + 00	0.2182E + 00	0.2204E + 00	0.2521E + 00
0.15E + 02	0.2038E + 00	0.1976E + 00	0.1998E + 00	0.2349E + 00
0.16E + 02	0.1855E + 00	0.1785E + 00	0.1807E + 00	0.2182E + 00
0.17E + 02	0.1686E + 00	0.1613E + 00	0.1633E + 00	0.2019E + 00
0.18E + 02	0.1532E + 00	0.1455E + 00	0.1474E + 00	0.1866E + 00

Table 2. (Continued)

x (per nm)	Lucite	Lexan	Kapton	Water
0.19E + 02	0.1393E + 00	0.1315E + 00	0.1333E + 00	0.1722E + 00
0.20E + 02	0.1266E + 00	0.1188E + 00	0.1204E + 00	0.1588E + 00
0.22E + 02	0.1046E + 00	0.9717E − 01	0.9852E − 01	0.1343E + 00
0.24E + 02	0.8671E − 01	0.7981E − 01	0.8093E − 01	0.1135E + 00
0.25E + 02	0.7904E − 01	0.7244E − 01	0.7346E − 01	0.1044E + 00
0.26E + 02	0.7211E − 01	0.6582E − 01	0.6675E − 01	0.9596E − 01
0.28E + 02	0.6021E − 01	0.5456E − 01	0.5533E − 01	0.8124E − 01
0.30E + 02	0.5049E − 01	0.4547E − 01	0.4611E − 01	0.6891E − 01
0.33E + 02	0.3909E − 01	0.3492E − 01	0.3540E − 01	0.5412E − 01
0.35E + 02	0.3313E − 01	0.2945E − 01	0.2985E − 01	0.4625E − 01
0.36E + 02	0.3055E − 01	0.2710E − 01	0.2747E − 01	0.4281E − 01
0.39E + 02	0.2415E − 01	0.2131E − 01	0.2159E − 01	0.3414E − 01
0.40E + 02	0.2239E − 01	0.1972E − 01	0.1998E − 01	0.3172E − 01
0.42E + 02	0.1929E − 01	0.1694E − 01	0.1716E − 01	0.2747E − 01
0.46E + 02	0.1449E − 01	0.1266E − 01	0.1282E − 01	0.2081E − 01
0.50E + 02	0.1105E − 01	0.9616E − 02	0.9729E − 02	0.1597E − 01
0.54E + 02	0.8550E − 02	0.7413E − 02	0.7497E − 02	0.1242E − 01
0.55E + 02	0.8034E − 02	0.6961E − 02	0.7039E − 02	0.1168E − 01
0.58E + 02	0.6698E − 02	0.5791E − 02	0.5855E − 02	0.9770E − 02
0.60E + 02	0.5956E − 02	0.5143E − 02	0.5198E − 02	0.8704E − 02
0.62E + 02	0.5311E − 02	0.4581E − 02	0.4630E − 02	0.7775E − 02
0.66E + 02	0.4260E − 02	0.3666E − 02	0.3705E − 02	0.6253E − 02
0.70E + 02	0.3452E − 02	0.2966E − 02	0.2996E − 02	0.5080E − 02
0.74E + 02	0.2823E − 02	0.2422E − 02	0.2447E − 02	0.4163E − 02
0.80E + 02	0.2123E − 02	0.1818E − 02	0.1836E − 02	0.3138E − 02
0.90E + 02	0.1371E − 02	0.1172E − 02	0.1183E − 02	0.2034E − 02
0.10E + 03	0.9227E − 03	0.7870E − 03	0.7942E − 03	0.1372E − 02
0.11E + 03	0.6425E − 03	0.5474E − 03	0.5522E − 03	0.9568E − 03
0.12E + 03	0.4604E − 03	0.3918E − 03	0.3953E − 03	0.6865E − 03
0.14E + 03	0.2540E − 03	0.2159E − 03	0.2177E − 03	0.3796E − 03
0.16E + 03	0.1512E − 03	0.1284E − 03	0.1294E − 03	0.2262E − 03
0.18E + 03	0.9546E − 04	0.8099E − 04	0.8165E − 04	0.1429E − 03
0.20E + 03	0.6318E − 04	0.5357E − 04	0.5400E − 04	0.9469E − 04
0.22E + 03	0.4346E − 04	0.3684E − 04	0.3713E − 04	0.6517E − 04
0.25E + 03	0.2629E − 04	0.2227E − 04	0.2245E − 04	0.3944E − 04
0.28E + 03	0.1682E − 04	0.1425E − 04	0.1436E − 04	0.2526E − 04
0.31E + 03	0.1126E − 04	0.9536E − 05	0.9611E − 05	0.1692E − 04
0.35E + 03	0.6980E − 05	0.5907E − 05	0.5953E − 05	0.1049E − 04
0.40E + 03	0.4124E − 05	0.3488E − 05	0.3515E − 05	0.6199E − 05
0.45E + 03	0.2592E − 05	0.2192E − 05	0.2208E − 05	0.3897E − 05
0.50E + 03	0.1712E − 05	0.1447E − 05	0.1458E − 05	0.2575E − 05
0.70E + 03	0.4561E − 06	0.3852E − 06	0.3881E − 06	0.6869E − 06
0.10E + 04	0.1130E − 06	0.9534E − 07	0.9603E − 07	0.1705E − 06
0.10E + 05	0.2127E − 10	0.1767E − 10	0.1774E − 10	0.3273E − 10
0.10E + 08	0.1126E − 19	0.9192E − 20	0.9197E − 20	0.1769E − 19
0.10E + 11	0.1151E − 28	0.9383E − 29	0.9384E − 29	0.1809E − 28

beef samples appeared similar to each other and both showed some sharp peaks as if from diffraction in crystalline materials. Form factors for the adipose samples appear very different from water.

Human breast tissue had peaks corresponding to the peaks of water and adipose, which is consistent with the composition of breast tissue. Since this tissue was not fresh, the

Table 3. Molecular coherent scattering form factors.

x (per nm)	Pork fat	Beef fat	Pork muscle	Beef muscle
0.00E + 00	0.8004E + 00	0.9064E + 00	0.5871E + 00	0.5871E + 00
0.10E + 00	0.8004E + 00	0.9064E + 00	0.5871E + 00	0.5871E + 00
0.20E + 00	0.8004E + 00	0.9064E + 00	0.5871E + 00	0.5871E + 00
0.30E + 00	0.8004E + 00	0.9064E + 00	0.5871E + 00	0.5871E + 00
0.40E + 00	0.8004E + 00	0.9064E + 00	0.5871E + 00	0.5871E + 00
0.50E + 00	0.8798E + 00	0.9746E + 00	0.5871E + 00	0.5871E + 00
0.60E + 00	0.1075E + 01	0.1097E + 01	0.5871E + 00	0.5871E + 00
0.70E + 00	0.1128E + 01	0.1178E + 01	0.5871E + 00	0.5871E + 00
0.80E + 00	0.1224E + 01	0.1287E + 01	0.5871E + 00	0.5871E + 00
0.90E + 00	0.1499E + 01	0.1555E + 01	0.5871E + 00	0.5871E + 00
0.10E + 01	0.1991E + 01	0.2043E + 01	0.9541E + 00	0.1012E + 01
0.11E + 01	0.2486E + 01	0.2555E + 01	0.1178E + 01	0.1208E + 01
0.12E + 01	0.2533E + 01	0.2166E + 01	0.1330E + 01	0.1381E + 01
0.13E + 01	0.1871E + 01	0.1878E + 01	0.1461E + 01	0.1514E + 01
0.14E + 01	0.1467E + 01	0.1537E + 01	0.1593E + 01	0.1643E + 01
0.15E + 01	0.1328E + 01	0.1439E + 01	0.1725E + 01	0.1749E + 01
0.16E + 01	0.1248E + 01	0.1382E + 01	0.1745E + 01	0.1769E + 01
0.17E + 01	0.1187E + 01	0.1321E + 01	0.1714E + 01	0.1738E + 01
0.18E + 01	0.1121E + 01	0.1242E + 01	0.1634E + 01	0.1655E + 01
0.19E + 01	0.1109E + 01	0.1211E + 01	0.1559E + 01	0.1572E + 01
0.20E + 01	0.1116E + 01	0.1195E + 01	0.1503E + 01	0.1518E + 01
0.22E + 01	0.1141E + 01	0.1211E + 01	0.1473E + 01	0.1490E + 01
0.24E + 01	0.1107E + 01	0.1165E + 01	0.1379E + 01	0.1377E + 01
0.25E + 01	0.1031E + 01	0.1085E + 01	0.1252E + 01	0.1253E + 01
0.26E + 01	0.9722E + 00	0.1007E + 01	0.1141E + 01	0.1138E + 01
0.28E + 01	0.8411E + 00	0.8671E + 00	0.9360E + 00	0.9311E + 00
0.30E + 01	0.7825E + 00	0.7884E + 00	0.8672E + 00	0.8658E + 00
0.32E + 01	0.7093E + 00	0.7303E + 00	0.8562E + 00	0.8438E + 00
0.34E + 01	0.6797E + 00	0.7212E + 00	0.8514E + 00	0.8479E + 00
0.35E + 01	0.6798E + 00	0.7111E + 00	0.8461E + 00	0.8294E + 00
0.36E + 01	0.6801E + 00	0.7064E + 00	0.8380E + 00	0.8237E + 00
0.38E + 01	0.6730E + 00	0.6999E + 00	0.8154E + 00	0.7957E + 00
0.40E + 01	0.6895E + 00	0.6996E + 00	0.7773E + 00	0.7615E + 00
0.42E + 01	0.6679E + 00	0.6837E + 00	0.7239E + 00	0.7127E + 00
0.44E + 01	0.6397E + 00	0.6478E + 00	0.6774E + 00	0.6638E + 00
0.45E + 01	0.6197E + 00	0.6207E + 00	0.6592E + 00	0.6483E + 00
0.46E + 01	0.6013E + 00	0.6076E + 00	0.6413E + 00	0.6273E + 00
0.48E + 01	0.5666E + 00	0.5704E + 00	0.5995E + 00	0.5944E + 00
0.50E + 01	0.5453E + 00	0.5436E + 00	0.5848E + 00	0.5755E + 00
0.55E + 01	0.4943E + 00	0.5036E + 00	0.5618E + 00	0.5568E + 00
0.60E + 01	0.4819E + 00	0.4840E + 00	0.5218E + 00	0.5188E + 00
0.65E + 01	0.4839E + 00	0.4863E + 00	0.4909E + 00	0.4848E + 00
0.70E + 01	0.4677E + 00	0.4719E + 00	0.4686E + 00	0.4628E + 00
0.80E + 01	0.4290E + 00	0.4332E + 00	0.4346E + 00	0.4214E + 00
0.90E + 01	0.3634E + 00	0.3658E + 00	0.3947E + 00	0.3884E + 00
0.10E + 02	0.3084E + 00	0.3084E + 00	0.3310E + 00	0.3310E + 00
0.11E + 02	0.2837E + 00	0.2837E + 00	0.3102E + 00	0.3102E + 00
0.12E + 02	0.2601E + 00	0.2601E + 00	0.2901E + 00	0.2901E + 00
0.13E + 02	0.2377E + 00	0.2377E + 00	0.2705E + 00	0.2705E + 00
0.14E + 02	0.2165E + 00	0.2165E + 00	0.2514E + 00	0.2514E + 00
0.15E + 02	0.1972E + 00	0.1972E + 00	0.2331E + 00	0.2331E + 00
0.16E + 02	0.1791E + 00	0.1791E + 00	0.2156E + 00	0.2156E + 00
0.17E + 02	0.1626E + 00	0.1626E + 00	0.1987E + 00	0.1987E + 00
0.18E + 02	0.1474E + 00	0.1474E + 00	0.1830E + 00	0.1830E + 00

Table 3. (Continued)

x (per nm)	Pork fat	Beef fat	Pork muscle	Beef muscle
0.19E + 02	0.1338E + 00	0.1338E + 00	0.1684E + 00	0.1684E + 00
0.20E + 02	0.1215E + 00	0.1215E + 00	0.1548E + 00	0.1548E + 00
0.22E + 02	0.1001E + 00	0.1001E + 00	0.1303E + 00	0.1303E + 00
0.24E + 02	0.8281E − 01	0.8281E − 01	0.1097E + 00	0.1097E + 00
0.25E + 02	0.7541E − 01	0.7541E − 01	0.1007E + 00	0.1007E + 00
0.26E + 02	0.6873E − 01	0.6873E − 01	0.9246E − 01	0.9246E − 01
0.28E + 02	0.5729E − 01	0.5729E − 01	0.7807E − 01	0.7807E − 01
0.30E + 02	0.4798E − 01	0.4798E − 01	0.6608E − 01	0.6608E − 01
0.33E + 02	0.3708E − 01	0.3708E − 01	0.5176E − 01	0.5176E − 01
0.35E + 02	0.3139E − 01	0.3139E − 01	0.4417E − 01	0.4417E − 01
0.36E + 02	0.2893E − 01	0.2893E − 01	0.4085E − 01	0.4085E − 01
0.39E + 02	0.2285E − 01	0.2285E − 01	0.3253E − 01	0.3253E − 01
0.40E + 02	0.2117E − 01	0.2117E − 01	0.3021E − 01	0.3021E − 01
0.42E + 02	0.1823E − 01	0.1823E − 01	0.2614E − 01	0.2614E − 01
0.46E + 02	0.1368E − 01	0.1368E − 01	0.1977E − 01	0.1977E − 01
0.50E + 02	0.1042E − 01	0.1042E − 01	0.1516E − 01	0.1516E − 01
0.54E + 02	0.8057E − 02	0.8057E − 02	0.1178E − 01	0.1178E − 01
0.55E + 02	0.7570E − 02	0.7570E − 02	0.1108E − 01	0.1108E − 01
0.58E + 02	0.6308E − 02	0.6308E − 02	0.9257E − 02	0.9257E − 02
0.60E + 02	0.5608E − 02	0.5608E − 02	0.8244E − 02	0.8244E − 02
0.62E + 02	0.4999E − 02	0.4999E − 02	0.7362E − 02	0.7362E − 02
0.66E + 02	0.4008E − 02	0.4008E − 02	0.5918E − 02	0.5918E − 02
0.70E + 02	0.3247E − 02	0.3247E − 02	0.4805E − 02	0.4805E − 02
0.74E + 02	0.2655E − 02	0.2655E − 02	0.3937E − 02	0.3937E − 02
0.80E + 02	0.1995E − 02	0.1995E − 02	0.2966E − 02	0.2966E − 02
0.90E + 02	0.1288E − 02	0.1288E − 02	0.1921E − 02	0.1921E − 02
0.10E + 03	0.8665E − 03	0.8665E − 03	0.1295E − 02	0.1295E − 02
0.11E + 03	0.6032E − 03	0.6032E − 03	0.9032E − 03	0.9032E − 03
0.12E + 03	0.4322E − 03	0.4322E − 03	0.6480E − 03	0.6480E − 03
0.14E + 03	0.2384E − 03	0.2384E − 03	0.3581E − 03	0.3581E − 03
0.16E + 03	0.1418E − 03	0.1418E − 03	0.2134E − 03	0.2134E − 03
0.18E + 03	0.8954E − 04	0.8954E − 04	0.1348E − 03	0.1348E − 03
0.20E + 03	0.5926E − 04	0.5926E − 04	0.8929E − 04	0.8929E − 04
0.22E + 03	0.4076E − 04	0.4076E − 04	0.6145E − 04	0.6145E − 04
0.25E + 03	0.2465E − 04	0.2465E − 04	0.3718E − 04	0.3718E − 04
0.28E + 03	0.1578E − 04	0.1578E − 04	0.2381E − 04	0.2381E − 04
0.31E + 03	0.1056E − 04	0.1056E − 04	0.1595E − 04	0.1595E − 04
0.35E + 03	0.6544E − 05	0.6544E − 05	0.9884E − 05	0.9884E − 05
0.40E + 03	0.3866E − 05	0.3866E − 05	0.5842E − 05	0.5842E − 05
0.45E + 03	0.2429E − 05	0.2429E − 05	0.3672E − 05	0.3672E − 05
0.50E + 03	0.1605E − 05	0.1605E − 05	0.2427E − 05	0.2427E − 05
0.70E + 03	0.4274E − 06	0.4274E − 06	0.6472E − 06	0.6472E − 06
0.10E + 04	0.1059E − 06	0.1059E − 06	0.1606E − 06	0.1606E − 06
0.10E + 05	0.1987E − 10	0.1987E − 10	0.3072E − 10	0.3072E − 10
0.10E + 08	0.1048E − 19	0.1048E − 19	0.1655E − 19	0.1655E − 19
0.10E + 11	0.1071E − 28	0.1071E − 28	0.1692E − 28	0.1692E − 28

question of how formaline affects the measured form factor arises. The form factor for formaline was measured separately and it appears very similar to that of water (which is 90% of formaline). Since formaline is mostly water and it replaces water in the tissue, the overall form factor of the breast tissue should not be changed too much by the presence of

Table 4. Molecular coherent scattering form factors.

x (per nm)	Pork kidney	Beef kidney	Pork liver	Beef liver
0.00E + 00	0.5871E + 00	0.5871E + 00	0.5871E + 00	0.5871E + 00
0.10E + 00	0.5871E + 00	0.5871E + 00	0.5871E + 00	0.5871E + 00
0.20E + 00	0.5871E + 00	0.5871E + 00	0.5871E + 00	0.5871E + 00
0.30E + 00	0.5871E + 00	0.5871E + 00	0.5871E + 00	0.5871E + 00
0.40E + 00	0.5871E + 00	0.5871E + 00	0.5871E + 00	0.5871E + 00
0.50E + 00	0.5871E + 00	0.5871E + 00	0.5871E + 00	0.5871E + 00
0.60E + 00	0.5871E + 00	0.5871E + 00	0.5871E + 00	0.5871E + 00
0.70E + 00	0.5871E + 00	0.5871E + 00	0.5871E + 00	0.5871E + 00
0.80E + 00	0.5871E + 00	0.5871E + 00	0.5871E + 00	0.5871E + 00
0.90E + 00	0.5871E + 00	0.5871E + 00	0.5871E + 00	0.5871E + 00
0.10E + 01	0.9287E + 00	0.9711E + 00	0.1082E + 01	0.1104E + 01
0.11E + 01	0.1144E + 01	0.1173E + 01	0.1284E + 01	0.1296E + 01
0.12E + 01	0.1305E + 01	0.1328E + 01	0.1422E + 01	0.1427E + 01
0.13E + 01	0.1472E + 01	0.1481E + 01	0.1502E + 01	0.1514E + 01
0.14E + 01	0.1624E + 01	0.1656E + 01	0.1649E + 01	0.1663E + 01
0.15E + 01	0.1785E + 01	0.1799E + 01	0.1775E + 01	0.1790E + 01
0.16E + 01	0.1830E + 01	0.1831E + 01	0.1795E + 01	0.1797E + 01
0.17E + 01	0.1779E + 01	0.1775E + 01	0.1743E + 01	0.1759E + 01
0.18E + 01	0.1712E + 01	0.1707E + 01	0.1667E + 01	0.1683E + 01
0.19E + 01	0.1633E + 01	0.1630E + 01	0.1595E + 01	0.1616E + 01
0.20E + 01	0.1562E + 01	0.1564E + 01	0.1528E + 01	0.1544E + 01
0.22E + 01	0.1534E + 01	0.1515E + 01	0.1486E + 01	0.1498E + 01
0.24E + 01	0.1421E + 01	0.1404E + 01	0.1368E + 01	0.1389E + 01
0.25E + 01	0.1296E + 01	0.1294E + 01	0.1261E + 01	0.1267E + 01
0.26E + 01	0.1157E + 01	0.1153E + 01	0.1136E + 01	0.1143E + 01
0.28E + 01	0.9574E + 00	0.9529E + 00	0.9450E + 00	0.9613E + 00
0.30E + 01	0.8881E + 00	0.8805E + 00	0.8790E + 00	0.8867E + 00
0.32E + 01	0.8613E + 00	0.8580E + 00	0.8399E + 00	0.8557E + 00
0.34E + 01	0.8670E + 00	0.8657E + 00	0.8461E + 00	0.8647E + 00
0.35E + 01	0.8661E + 00	0.8642E + 00	0.8404E + 00	0.8571E + 00
0.36E + 01	0.8603E + 00	0.8474E + 00	0.8328E + 00	0.8458E + 00
0.38E + 01	0.8209E + 00	0.8094E + 00	0.7891E + 00	0.8107E + 00
0.40E + 01	0.7736E + 00	0.7735E + 00	0.7706E + 00	0.7776E + 00
0.42E + 01	0.7225E + 00	0.7243E + 00	0.7163E + 00	0.7366E + 00
0.44E + 01	0.6783E + 00	0.6850E + 00	0.6670E + 00	0.6962E + 00
0.45E + 01	0.6458E + 00	0.6471E + 00	0.6456E + 00	0.6625E + 00
0.46E + 01	0.6258E + 00	0.6304E + 00	0.6183E + 00	0.6416E + 00
0.48E + 01	0.5935E + 00	0.5945E + 00	0.5724E + 00	0.5953E + 00
0.50E + 01	0.5735E + 00	0.5751E + 00	0.5673E + 00	0.5829E + 00
0.55E + 01	0.5547E + 00	0.5532E + 00	0.5470E + 00	0.5574E + 00
0.60E + 01	0.5190E + 00	0.5217E + 00	0.5092E + 00	0.5255E + 00
0.65E + 01	0.4823E + 00	0.4806E + 00	0.4792E + 00	0.4827E + 00
0.70E + 01	0.4646E + 00	0.4702E + 00	0.4631E + 00	0.4687E + 00
0.80E + 01	0.4285E + 00	0.4330E + 00	0.4300E + 00	0.4353E + 00
0.90E + 01	0.3902E + 00	0.3863E + 00	0.3853E + 00	0.3976E + 00
0.10E + 02	0.3275E + 00	0.3275E + 00	0.3285E + 00	0.3285E + 00
0.11E + 02	0.3064E + 00	0.3064E + 00	0.3070E + 00	0.3070E + 00
0.12E + 02	0.2861E + 00	0.2861E + 00	0.2865E + 00	0.2865E + 00
0.13E + 02	0.2665E + 00	0.2665E + 00	0.2667E + 00	0.2667E + 00
0.14E + 02	0.2476E + 00	0.2476E + 00	0.2477E + 00	0.2477E + 00
0.15E + 02	0.2295E + 00	0.2295E + 00	0.2295E + 00	0.2295E + 00
0.16E + 02	0.2123E + 00	0.2123E + 00	0.2122E + 00	0.2122E + 00
0.17E + 02	0.1958E + 00	0.1958E + 00	0.1957E + 00	0.1957E + 00
0.18E + 02	0.1804E + 00	0.1804E + 00	0.1803E + 00	0.1803E + 00

Table 4. (Continued)

x (per nm)	Pork kidney	Beef kidney	Pork liver	Beef liver
0.19E + 02	0.1661E + 00	0.1661E + 00	0.1660E + 00	0.1660E + 00
0.20E + 02	0.1529E + 00	0.1529E + 00	0.1528E + 00	0.1528E + 00
0.22E + 02	0.1290E + 00	0.1290E + 00	0.1291E + 00	0.1291E + 00
0.24E + 02	0.1091E + 00	0.1091E + 00	0.1092E + 00	0.1092E + 00
0.25E + 02	0.1003E + 00	0.1003E + 00	0.1005E + 00	0.1005E + 00
0.26E + 02	0.9232E − 01	0.9232E − 01	0.9251E − 01	0.9251E − 01
0.28E + 02	0.7838E − 01	0.7838E − 01	0.7864E − 01	0.7864E − 01
0.30E + 02	0.6678E − 01	0.6678E − 01	0.6710E − 01	0.6710E − 01
0.33E + 02	0.5292E − 01	0.5292E − 01	0.5331E − 01	0.5331E − 01
0.35E + 02	0.4557E − 01	0.4557E − 01	0.4599E − 01	0.4599E − 01
0.36E + 02	0.4236E − 01	0.4236E − 01	0.4279E − 01	0.4279E − 01
0.39E + 02	0.3427E − 01	0.3427E − 01	0.3472E − 01	0.3472E − 01
0.40E + 02	0.3202E − 01	0.3202E − 01	0.3247E − 01	0.3247E − 01
0.42E + 02	0.2803E − 01	0.2803E − 01	0.2849E − 01	0.2849E − 01
0.46E + 02	0.2176E − 01	0.2176E − 01	0.2220E − 01	0.2220E − 01
0.50E + 02	0.1715E − 01	0.1715E − 01	0.1756E − 01	0.1756E − 01
0.54E + 02	0.1371E − 01	0.1371E − 01	0.1409E − 01	0.1409E − 01
0.55E + 02	0.1299E − 01	0.1299E − 01	0.1336E − 01	0.1336E − 01
0.58E + 02	0.1110E − 01	0.1110E − 01	0.1144E − 01	0.1144E − 01
0.60E + 02	0.1003E − 01	0.1003E − 01	0.1035E − 01	0.1035E − 01
0.62E + 02	0.9092E − 02	0.9092E − 02	0.9390E − 02	0.9390E − 02
0.66E + 02	0.7519E − 02	0.7519E − 02	0.7782E − 02	0.7782E − 02
0.70E + 02	0.6276E − 02	0.6276E − 02	0.6506E − 02	0.6506E − 02
0.74E + 02	0.5280E − 02	0.5280E − 02	0.5481E − 02	0.5481E − 02
0.80E + 02	0.4128E − 02	0.4128E − 02	0.4292E − 02	0.4292E − 02
0.90E + 02	0.2825E − 02	0.2825E − 02	0.2942E − 02	0.2942E − 02
0.10E + 03	0.1996E − 02	0.1996E − 02	0.2080E − 02	0.2080E − 02
0.11E + 03	0.1447E − 02	0.1447E − 02	0.1508E − 02	0.1508E − 02
0.12E + 03	0.1073E − 02	0.1073E − 02	0.1118E − 02	0.1118E − 02
0.14E + 03	0.6245E − 03	0.6245E − 03	0.6504E − 03	0.6504E − 03
0.16E + 03	0.3864E − 03	0.3864E − 03	0.4021E − 03	0.4021E − 03
0.18E + 03	0.2512E − 03	0.2512E − 03	0.2612E − 03	0.2612E − 03
0.20E + 03	0.1701E − 03	0.1701E − 03	0.1768E − 03	0.1768E − 03
0.22E + 03	0.1191E − 03	0.1191E − 03	0.1237E − 03	0.1237E − 03
0.25E + 03	0.7358E − 04	0.7358E − 04	0.7639E − 04	0.7639E − 04
0.28E + 03	0.4786E − 04	0.4786E − 04	0.4966E − 04	0.4966E − 04
0.31E + 03	0.3246E − 04	0.3246E − 04	0.3367E − 04	0.3367E − 04
0.35E + 03	0.2040E − 04	0.2040E − 04	0.2115E − 04	0.2115E − 04
0.40E + 03	0.1223E − 04	0.1223E − 04	0.1267E − 04	0.1267E − 04
0.45E + 03	0.7774E − 05	0.7774E − 05	0.8054E − 05	0.8054E − 05
0.50E + 03	0.5186E − 05	0.5186E − 05	0.5371E − 05	0.5371E − 05
0.70E + 03	0.1426E − 05	0.1426E − 05	0.1476E − 05	0.1476E − 05
0.10E + 04	0.3668E − 06	0.3668E − 06	0.3789E − 06	0.3789E − 06
0.10E + 05	0.1034E − 09	0.1034E − 09	0.1058E − 09	0.1058E − 09
0.10E + 08	0.8282E − 19	0.8282E − 19	0.8363E − 19	0.8363E − 19
0.10E + 11	0.9385E − 28	0.9385E − 28	0.9412E − 28	0.9412E − 28

formaline. In fact, a sum of the form factors of about one part water and two parts beef adipose gives a shape very similar to that measured for the breast tissue form factor.

Some work is needed to improve the data collection, especially in the low-angle range where the effects of the sample container are strong. For example, some of the materials, like water and beef blood, had a slight but noticeable inward curvature of the Kapton film

Table 5. Molecular coherent scattering form factors.

x (per nm)	Pork heart	Beef blood	Breast tissue	Formaline
0.00E + 00	0.5871E + 00	0.5871E + 00	0.8191E + 00	0.5871E + 00
0.10E + 00	0.5871E + 00	0.5871E + 00	0.8191E + 00	0.5871E + 00
0.20E + 00	0.5871E + 00	0.5871E + 00	0.8191E + 00	0.5871E + 00
0.30E + 00	0.5871E + 00	0.5871E + 00	0.8191E + 00	0.5871E + 00
0.40E + 00	0.5871E + 00	0.5871E + 00	0.8191E + 00	0.5871E + 00
0.50E + 00	0.5871E + 00	0.5871E + 00	0.9665E + 00	0.5871E + 00
0.60E + 00	0.5871E + 00	0.5871E + 00	0.1134E + 01	0.5871E + 00
0.70E + 00	0.5871E + 00	0.5871E + 00	0.1250E + 01	0.5871E + 00
0.80E + 00	0.5871E + 00	0.5871E + 00	0.1247E + 01	0.5871E + 00
0.90E + 00	0.5871E + 00	0.5871E + 00	0.1464E + 01	0.5871E + 00
0.10E + 01	0.9336E + 00	0.5871E + 00	0.1813E + 01	0.6872E + 00
0.11E + 01	0.1124E + 01	0.6910E + 00	0.2073E + 01	0.8685E + 00
0.12E + 01	0.1322E + 01	0.9595E + 00	0.1890E + 01	0.1118E + 01
0.13E + 01	0.1504E + 01	0.1227E + 01	0.1706E + 01	0.1307E + 01
0.14E + 01	0.1672E + 01	0.1445E + 01	0.1670E + 01	0.1563E + 01
0.15E + 01	0.1844E + 01	0.1649E + 01	0.1710E + 01	0.1782E + 01
0.16E + 01	0.1878E + 01	0.1723E + 01	0.1708E + 01	0.1836E + 01
0.17E + 01	0.1831E + 01	0.1695E + 01	0.1648E + 01	0.1792E + 01
0.18E + 01	0.1759E + 01	0.1625E + 01	0.1553E + 01	0.1685E + 01
0.19E + 01	0.1657E + 01	0.1551E + 01	0.1486E + 01	0.1585E + 01
0.20E + 01	0.1594E + 01	0.1488E + 01	0.1438E + 01	0.1546E + 01
0.22E + 01	0.1550E + 01	0.1463E + 01	0.1409E + 01	0.1500E + 01
0.24E + 01	0.1426E + 01	0.1350E + 01	0.1323E + 01	0.1416E + 01
0.25E + 01	0.1317E + 01	0.1235E + 01	0.1220E + 01	0.1285E + 01
0.26E + 01	0.1161E + 01	0.1110E + 01	0.1096E + 01	0.1150E + 01
0.28E + 01	0.9638E + 00	0.9187E + 00	0.9061E + 00	0.9281E + 00
0.30E + 01	0.8914E + 00	0.8455E + 00	0.8443E + 00	0.8622E + 00
0.32E + 01	0.8656E + 00	0.8215E + 00	0.7942E + 00	0.8381E + 00
0.34E + 01	0.8732E + 00	0.8178E + 00	0.7964E + 00	0.8336E + 00
0.35E + 01	0.8670E + 00	0.8074E + 00	0.7930E + 00	0.8275E + 00
0.36E + 01	0.8604E + 00	0.8009E + 00	0.8021E + 00	0.8289E + 00
0.38E + 01	0.8249E + 00	0.7608E + 00	0.7664E + 00	0.7831E + 00
0.40E + 01	0.7809E + 00	0.7069E + 00	0.7370E + 00	0.7280E + 00
0.42E + 01	0.7299E + 00	0.6410E + 00	0.7095E + 00	0.6729E + 00
0.44E + 01	0.6866E + 00	0.5978E + 00	0.6654E + 00	0.6083E + 00
0.45E + 01	0.6546E + 00	0.5654E + 00	0.6406E + 00	0.5825E + 00
0.46E + 01	0.6339E + 00	0.5507E + 00	0.6119E + 00	0.5478E + 00
0.48E + 01	0.6047E + 00	0.5272E + 00	0.5851E + 00	0.5279E + 00
0.50E + 01	0.5848E + 00	0.5018E + 00	0.5654E + 00	0.5104E + 00
0.55E + 01	0.5632E + 00	0.4929E + 00	0.5441E + 00	0.5087E + 00
0.60E + 01	0.5228E + 00	0.4649E + 00	0.5133E + 00	0.4673E + 00
0.65E + 01	0.4808E + 00	0.4264E + 00	0.4889E + 00	0.4282E + 00
0.70E + 01	0.4664E + 00	0.4100E + 00	0.4722E + 00	0.4093E + 00
0.80E + 01	0.4317E + 00	0.3746E + 00	0.4282E + 00	0.3793E + 00
0.90E + 01	0.3849E + 00	0.3375E + 00	0.3967E + 00	0.3450E + 00
0.10E + 02	0.3273E + 00	0.3275E + 00	0.3144E + 00	0.3230E + 00
0.11E + 02	0.3061E + 00	0.3067E + 00	0.2921E + 00	0.3028E + 00
0.12E + 02	0.2858E + 00	0.2867E + 00	0.2707E + 00	0.2833E + 00
0.13E + 02	0.2661E + 00	0.2673E + 00	0.2502E + 00	0.2643E + 00
0.14E + 02	0.2471E + 00	0.2485E + 00	0.2305E + 00	0.2457E + 00
0.15E + 02	0.2290E + 00	0.2305E + 00	0.2121E + 00	0.2280E + 00
0.16E + 02	0.2117E + 00	0.2133E + 00	0.1947E + 00	0.2109E + 00
0.17E + 02	0.1952E + 00	0.1968E + 00	0.1784E + 00	0.1945E + 00
0.18E + 02	0.1799E + 00	0.1814E + 00	0.1633E + 00	0.1792E + 00

Table 5. (Continued)

x (per nm)	Pork heart	Beef blood	Breast tissue	Formaline
0.19E + 02	0.1656E + 00	0.1671E + 00	0.1495E + 00	0.1649E + 00
0.20E + 02	0.1524E + 00	0.1538E + 00	0.1367E + 00	0.1517E + 00
0.22E + 02	0.1286E + 00	0.1299E + 00	0.1142E + 00	0.1278E + 00
0.24E + 02	0.1087E + 00	0.1098E + 00	0.9556E − 01	0.1077E + 00
0.25E + 02	0.9995E − 01	0.1009E + 00	0.8746E − 01	0.9884E − 01
0.26E + 02	0.9198E − 01	0.9289E − 01	0.8010E − 01	0.9077E − 01
0.28E + 02	0.7809E − 01	0.7883E − 01	0.6734E − 01	0.7667E − 01
0.30E + 02	0.6654E − 01	0.6712E − 01	0.5679E − 01	0.6493E − 01
0.33E + 02	0.5274E − 01	0.5312E − 01	0.4429E − 01	0.5088E − 01
0.35E + 02	0.4543E − 01	0.4569E − 01	0.3769E − 01	0.4343E − 01
0.36E + 02	0.4223E − 01	0.4245E − 01	0.3483E − 01	0.4018E − 01
0.39E + 02	0.3418E − 01	0.3427E − 01	0.2766E − 01	0.3200E − 01
0.40E + 02	0.3194E − 01	0.3199E − 01	0.2567E − 01	0.2973E − 01
0.42E + 02	0.2797E − 01	0.2797E − 01	0.2218E − 01	0.2572E − 01
0.46E + 02	0.2173E − 01	0.2164E − 01	0.1673E − 01	0.1946E − 01
0.50E + 02	0.1714E − 01	0.1699E − 01	0.1281E − 01	0.1493E − 01
0.54E + 02	0.1371E − 01	0.1353E − 01	0.9931E − 02	0.1160E − 01
0.55E + 02	0.1300E − 01	0.1281E − 01	0.9338E − 02	0.1091E − 01
0.58E + 02	0.1111E − 01	0.1091E − 01	0.7798E − 02	0.9119E − 02
0.60E + 02	0.1004E − 01	0.9844E − 02	0.6941E − 02	0.8121E − 02
0.62E + 02	0.9102E − 02	0.8902E − 02	0.6195E − 02	0.7253E − 02
0.66E + 02	0.7531E − 02	0.7335E − 02	0.4976E − 02	0.5831E − 02
0.70E + 02	0.6288E − 02	0.6100E − 02	0.4038E − 02	0.4735E − 02
0.74E + 02	0.5291E − 02	0.5114E − 02	0.3306E − 02	0.3880E − 02
0.80E + 02	0.4137E − 02	0.3979E − 02	0.2489E − 02	0.2924E − 02
0.90E + 02	0.2832E − 02	0.2704E − 02	0.1611E − 02	0.1894E − 02
0.10E + 03	0.2000E − 02	0.1900E − 02	0.1085E − 02	0.1277E − 02
0.11E + 03	0.1450E − 02	0.1370E − 02	0.7564E − 03	0.8905E − 03
0.12E + 03	0.1075E − 02	0.1012E − 02	0.5424E − 03	0.6389E − 03
0.14E + 03	0.6249E − 03	0.5851E − 03	0.2996E − 03	0.3531E − 03
0.16E + 03	0.3864E − 03	0.3604E − 03	0.1785E − 03	0.2104E − 03
0.18E + 03	0.2510E − 03	0.2335E − 03	0.1127E − 03	0.1329E − 03
0.20E + 03	0.1699E − 03	0.1576E − 03	0.7464E − 04	0.8806E − 04
0.22E + 03	0.1189E − 03	0.1102E − 03	0.5136E − 04	0.6060E − 04
0.25E + 03	0.7343E − 04	0.6789E − 04	0.3108E − 04	0.3667E − 04
0.28E + 03	0.4775E − 04	0.4407E − 04	0.1990E − 04	0.2348E − 04
0.31E + 03	0.3238E − 04	0.2985E − 04	0.1332E − 04	0.1573E − 04
0.35E + 03	0.2034E − 04	0.1873E − 04	0.8257E − 05	0.9749E − 05
0.40E + 03	0.1218E − 04	0.1121E − 04	0.4880E − 05	0.5762E − 05
0.45E + 03	0.7746E − 05	0.7117E − 05	0.3067E − 05	0.3622E − 05
0.50E + 03	0.5166E − 05	0.4743E − 05	0.2027E − 05	0.2394E − 05
0.70E + 03	0.1420E − 05	0.1300E − 05	0.5403E − 06	0.6384E − 06
0.10E + 04	0.3646E − 06	0.3329E − 06	0.1340E − 06	0.1584E − 06
0.10E + 05	0.1021E − 09	0.9112E − 10	0.2550E − 10	0.3033E − 10
0.10E + 08	0.8100E − 19	0.7125E − 19	0.1366E − 19	0.1635E − 19
0.10E + 11	0.9134E − 28	0.7998E − 28	0.1397E − 28	0.1673E − 28

once they were loaded into the container. Other materials had a slight outward curvature of the Kapton film after loading. Care was taken to try to minimize these problems but they could not be completely eliminated. This and the changes in response caused by slight alignment changes led to problems at low values of x. The remedies presented in this paper to these problems are not rigorous and are somewhat cumbersome to use.

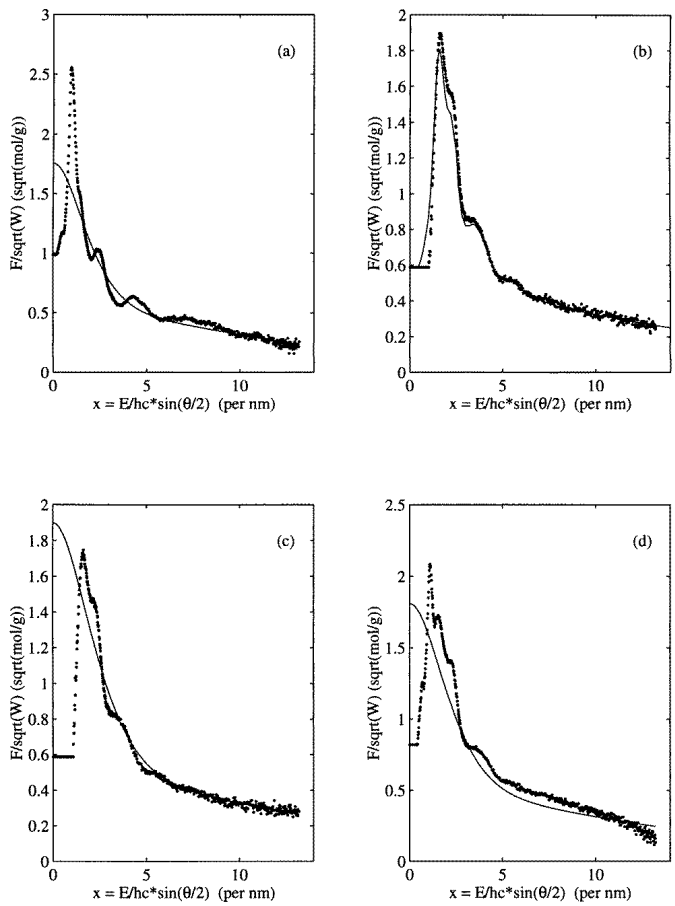

Figure 6. Free gas model (——) and the molecular coherent scattering form factor (·) reduced from scattering distribution measurements for (a) Lexan, (b) water (in this case, Narten's measurement is shown instead of the free gas model), (c) beef blood and (d) breast tissue.

It was assumed in this procedure that only the coherent scatter form factor was affected by intramolecular and intermolecular interferences. As in almost all reported literature, incoherent scatter for molecules was calculated using atomic scattering factors. However, Guy *et al* (1992) measured the incoherent scattering distributions of several metals and showed some differences compared with Hubbell's incoherent scattering factors. Their work implied that the incoherent scattering factors may need to include molecular and solid state electron binding effects. This is, however, not expected to be a significant error in the data presented since incoherent scatter is only a minor component, as shown in figure 2(c).

The molecular form factors of Lucite and pork adipose from this study and from Tartari *et al* (1997b), shown in figure 7, agree quite well given the different quality of beams and analysis techniques. The molecular form factors also agree in shape with other powder diffraction studies (Kosanetzky *et al* 1987, Evans *et al* 1991, Leliveld 1996). However, this study stands apart from others with its use of monoenergetic x-rays and its unique approach to extraction of the form factors using dual-energy measurements and detailed Monte Carlo modelling.

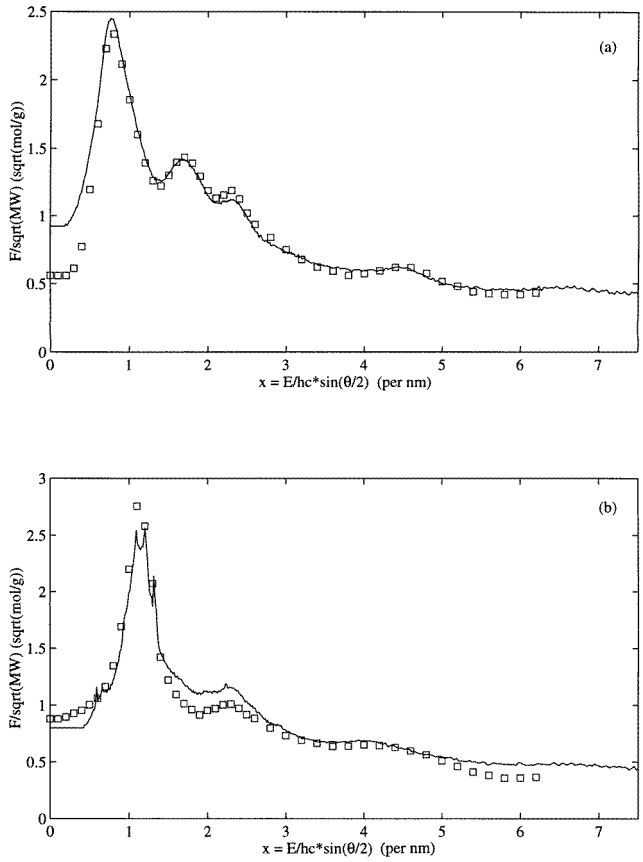

Figure 7. Molecular form factors for (a) Lucite and (b) pork adipose compared for this study (——) and Tartari *et al* (1997b) (□).

5. Summary

Molecular form factors were measured and tabulated for two plastics, five pork tissues, five beef tissues, water, Kapton, formaline and human breast tissue. The final values were constructed by combining measurements at two different source energies made with monoenergetic polarized synchrotron radiation. The x values listed in the tables match those of Hubbell and Øverbø's work and should be able to be easily implemented into codes.

We believe that these tables will be most useful to those in the medical physics community, especially in a low-energy application, such as mammographic imaging.

Acknowledgments

Research was carried out in part at the National Synchrotron Light Source, Brookhaven National Laboratory, which is supported by the US Department of Energy, Division of Materials Sciences and Division of Chemical Sciences. Many thanks to Dr Peter W Stephens for allowing this work to be done on beamline X3B1. Thanks also to Dr David Cox of beamline X7A where some preliminary measurements were made.

Monte Carlo simulations and the analysis of the experimental data were performed on a Sun Ultra 2/2200 donated by Sun Microsystems, through their Academic Equipment Grant. Many thanks to Sun Microsystems.

Financial support of the first author (DEP) was provided by Dr R Eugene Johnston, University of North Carolina, through his Breast Cancer Research Grant from the US Army Medical Research and Material Command.

Animal tissue samples were obtained from McLamb's Abattoir of Benson, NC.

References

Boone J M 1992 Parameterized x-ray absorption in diagnostic radiology from Monte Carlo calculations: implications for x-ray detector design *Med. Phys.* **19** 1467–73

Chan H P and Doi K 1983 Energy and angular dependence of x-ray absorption and its effect on radiographic response in screen-film systems *Phys. Med. Biol.* **28** 565–79

Chapman D, Thomlinson W, Johnston R E, Washburn D, Pisano E, Gmür N, Zhong Z, Menk R, Arfelli F and Sayers D 1997 Diffraction enhanced x-ray imaging *Phys. Med. Biol.* **42** 2015–25

Evans S H, Bradley D A, Dance D R, Bateman J E and Jones C H 1991 Measurement of small-angle photon scattering for some breast tissues and tissue substitute materials *Phys. Med. Biol.* **35** 7–18

Guy L P, Taylor R B and Whittingham I B 1992 Incoherent scattering function at small momentum transfer *Nucl. Instrum. Methods* B **69** 174–7

Hubbell J H and Øverbø I 1979 Relativistic atomic form factors and photon coherent cross sections *J. Phys. Chem. Ref. Data* **8** 69–105

Hubbell J H, Veigele W J, Briggs E A, Brown R T, Cromer D T and Howerton R J 1975 Atomic form factors, incoherent scattering functions, and photon cross sections *J. Phys. Chem. Ref. Data* **4** 471–538

——1977 Erratum: atomic form factors, incoherent scattering functions, and photon cross sections *J. Phys. Chem. Ref. Data* **6** 615–16

ICRU 1992 Photon, electron, proton, and neutron interaction data for body tissues *ICRU Report* 46 (Bethesda, MD: ICRU)

Johns P C and Yaffe M J 1983 Coherent scattering in diagnostic radiology *Med. Phys.* **10** 40-50

Johnston R E, Washburn D, Pisano E, Burns C, Thomlinson W, Chapman L D, Arfelli F, Gmür N F, Zhong Z and Sayers D E 1996 Mammographic phantom studies with synchrotron radiation *Radiology* **200** 659–63

Kosanetzky J, Knoerr B, Harding G and Neitzel U 1987 X-ray diffraction measurements of some plastic materials and body tissues *Med. Phys.* **14** 526–32

Leliveld C J, Maas J G, Bom V R and van Eijk C W E 1996 Monte Carlo modelling of coherent scattering: influence of interference *IEEE Trans. Nuc. Sci.* **43** 3315–21

Narten A H 1970 X-ray diffraction data on liquid water in the temperature range 4 to 200 °C *Report* ORNL-4578 (Oak Ridge, TN: Oak Ridge National Laboratory)

Narten A H and Levy H A 1971 Liquid water: molecular correlation functions from x-ray diffraction *J. Chem. Phys.* **55** 2263–9

Tartari A, Casnati E, Bonifazzi C and Baraldi C 1997b Molecular differential cross sections for x-ray coherent scattering in fat and polymethyl methacrylate *Phys. Med. Biol.* **42** 2551–60

Tartari A, Casnati E, Bonifazzi C and Paganetto G 1997a Photon scattering by compounds: an assessment of the validity of the independent atomic model approximation *X-Ray Spectrom.* **26** 169–73